nature communications

Article

https://doi.org/10.1038/s41467-025-63148-0

In-situ localised alignment assisted salting-out enhanced ionogels with high strength, toughness and impact resistance

Received: 17 February 2025

Accepted: 11 August 2025

Published online: 18 August 2025

Check for updates

Zhentao Zhang[1], Min Sang[1] ✉, Zimu Li[1], Yucheng Pan[1], Jianpeng Wu[1], Shilong Duan[1] & Xinglong Gong[1,2] ✉

Ionic gels have promise in a range of applications but are limited in extreme environments. Here, we report a method for preparation of an ionic gel with improved mechanical properties, through the formation of a micro-orientated structure and increased crystallisation and aggregation of polymer chains. The resulting ionic gels exhibit tunable mechanical properties, including high strength (18.1–62.2 MPa), toughness (56.8–123.7 MJ m^{-3}), modulus (18.8–187.8 MPa), and excellent impact resistance. These gels exhibit greater energy dissipation than Kevlar under comparable impact velocities. Molecular dynamics simulations reveal that the localised alignment assisted salting-out process enhances hydrogen bonding and chain interactions, improving structural stability. This strategy is also effective in other polymer systems, such as PAAM hydrogels, demonstrating broad applicability. Overall, this approach greatly enhances the mechanical and protective performance of ionic gels for demanding applications.

Ionic gels[1–4], known for their excellent conductivity, electrochemical stability, and non-volatility, have demonstrated broad application potential in fields such as flexible electronics, soft robotics, protective equipment, and aerospace[5–7]. However, traditional ionic gels often suffer from low mechanical strength and are prone to fracture, which limits their reliability in extreme environments. With increasingly complex application scenarios particularly in conditions involving extreme temperatures, high-impact forces, and intense vibrations-mechanical toughness has become a critical factor. These challenging conditions, commonly encountered in automotive safety, aerospace, and personal protective equipment, not only risk degrading equipment performance but may also directly threaten human safety. Therefore, enhancing the mechanical properties of ionic gels to meet the demands of these high-intensity and complex environments has become an urgent technical challenge[8–10]. Developing ionic gels with high toughness and impact resistance could bring greater reliability and safety to the next generation of flexible electronics and protective equipment.

Currently, strategies to enhance the toughness of high-performance ionic gels focus mainly on physical and chemical modifications to improve their mechanical properties. These methods include mechanical training[11–13], filler incorporation[14–16], and directional freezing[17–19]. For example, mechanical training applies external force during fabrication to induce ordered microstructures within the gel, thus improving its strength and fracture toughness. However, gels produced by mechanical training often show reduced stretchability, making them unsuitable for applications that require high extensibility. The Hofmeister effect[20–22], through the introduction of specific ions, can also induce more stable ionic and hydrogen bond networks between polymer chains, enhancing toughness and fatigue resistance while maintaining flexibility. For instance, He et al.[23] used a freeze-assisted salting-out treatment to create a layered polyvinyl alcohol (PVA) hydrogel structure with high anisotropy, containing micron-scale honeycomb walls connected by nanofiber networks. Inspired by biological systems, Gong et al.[24] applied confined drying to create hydrogels with perfectly aligned, multi-

[1]Department of Modern Mechanics, CAS Key Laboratory of Mechanical Behavior and Design of Materials, University of Science and Technology of China (USTC), Hefei, Anhui, PR China. [2]State Key Laboratory of Fire Science, University of Science and Technology of China (USTC), Hefei, Anhui, PR China. ✉e-mail: sm019050@mail.ustc.edu.cn; gongxl@ustc.edu.cn

scale fiber structures, yielding performance comparable to cartilage and tendons.

Most current studies use salt solutions for the salting-out process; in this study, however, we employ ionic liquids[25–27]. Ionic liquids offer greater ion-exchange capacity and thermal stability, forming a robust molecular network among polymer chains. By combining this with a localized alignment assisted salting-out technique, in which the organogel is fixed at both ends, we can restrict its freedom to shrink during the ionic liquid exchange, resulting in tensile stress along the gel's length. This process gradually stabilizes a highly ordered micro-oriented structure during salting-out. Additionally, the tensile stress promotes further aggregation and crystallization of PVA chains, ultimately leading to a highly entangled and micro-oriented structure. Unlike traditional salt solutions, ionic liquids offer greater ion-exchange capacity, better thermal stability, and the ability to form robust molecular networks among polymer chains. These features allow ionic liquids to produce gels with improved mechanical properties. However, the process can be limited by the tendency of ionic gels to shrink uncontrollably during salting-out, which leads to anisotropic stress distribution and compromises their uniformity and structural stability. Addressing these shortcomings requires innovative strategies to maintain structural order while harnessing the benefits of ionic liquids.

As a result, the highly strong and tough PVA ionic gel was developed by a synergistic strengthening strategy of in situ localized alignment and salting-out. The resulting ionic gels exhibit tunable strength (18.1–62.2 MPa), toughness (56.8–123.7 MJ m^{-3}), and modulus (18.8–187.8 MPa). More importantly, the PL-gel shows excellent protection against puncture damage, with a maximum puncture force of 139.7 ± 12.3 N and puncture energy of 2.6 ± 0.2 J/m. Under high-speed ballistic impact, the PL-gel achieves an extraordinary energy dissipation of 18.4 kJ m^{-1}, even exceeding Kevlar at similar impact velocities. Furthermore, molecular dynamics simulations reveal that localized alignment assisted salting-out strategy effectively increases the number of hydrogen bonds as well as strengthens the hydrogen bonds. This significantly suppresses the motion of the ethylene glycol network and enhances interactions between molecular chains, thereby improving the overall structural stability of polymer network. Finally, the generality of this toughening strategy is demonstrated by applying it to PAAM hydrogels, indicating the broad applicability of localized alignment assisted salting-out across different polymer matrices. The results show that this approach not only significantly improves the mechanical properties and anti-impact capability of ionic gels but also offers broad adaptability, opening possibilities for developing high-performance, impact-resistant materials towards advanced applications in flexible electronics, protective equipment, and beyond.

Results

Preparation and mechanical properties of PL-gel

Figure 1a illustrates the manufacturing process of high-strength and tough PVA ionic gel via in situ localized alignment and salting-out synergistic enhancement strategy, characterized by strong force-induced aggregation. Initially, ethylene glycol and polyvinyl alcohol (PVA) were heated to 130 °C and thoroughly mixed, then poured into a custom mold and frozen to obtain a preliminary organic gel. This organic gel was then fixed onto a polyurethane (PU) plate and immersed in an ionic liquid for ion exchange, resulting in the formation of the PL-gel. During this process, the ionic liquid replaces the ethylene glycol within the organic gel, enhancing the hydrophobic interactions between PVA chains and establishing strong three-dimensional supramolecular interactions among the polymer segments (Fig. 1b). As shown in Fig. 1c and Supplementary Fig. 1, the resulting PL-gel exhibits high transparency, with transmittance exceeding 90% across the visible light wavelength range (300–750 nm). Since both ends of the organic gel are fixed, its width and thickness contract while its length remains unchanged. This design limits the gel's free shrinkage during the replacement process, causing it to experience tensile stress along the length direction (Supplementary Fig. 2). As this tensile stress is applied, the physical cross-linking points between the molecular chains gradually align along the tensile direction, forming a more ordered micro-orientation structure. This micro-orientation is progressively established and stabilized during the salting-out process, preserving the gel's tensile strain. Ultimately, this in situ localized alignment assisted salting-out strategy leads to significant entanglement and micro-orientation of the PVA chains, endowing the ionic gel with high strength, toughness, and hardness. The synergistic effects of micro-orientation and entanglement allow PVA chains to achieve uniform orientation structures under tension, while the entanglement effect enhances stress transmission along the polymer chains, further improving the material's toughness. As shown in Supplementary Fig. 3, the PL-gel can withstand a load of 10 kg water bucket (58823 times its own weight) without damage, as well as can bear tensile, twisted, and knotted stretching, confirming its exceptional strength and toughness.

To further investigate the chemical structure of the PL-gel, Fourier-transform infrared (FT-IR) spectroscopy was conducted (Fig. 1d). The hydroxyl (O-H) stretching vibrations of ethylene glycol and PVA appear as broad and intense peaks around 3300 cm^{-1}, confirming the presence of hydroxyl functional groups within the gel network. The vibrational peak of 1-butyl-3-methylimidazolium tetrafluoroborate (IL) appears near 1570 cm^{-1}, and a similar peak is observed in the ion-exchanged PVA ionic gel, indicating that the ionic liquid has infiltrated into the ionic gel. EDS and XPS results further validate the introduction of the ionic liquid, with B and F peaks detected in both PL-gel and PD-gel (Fig. 1e and Supplementary Fig. 4). Moreover, EDS results show a uniform distribution of the characteristic elements F and B in the PL-gel (Supplementary Fig. 4). Besides, SEM images reveal a highly uniform microstructure of the PL-gel (Supplementary Fig. 5). To characterize the internal orientation structure of ionic gels, small-angle and wide-angle X-ray scattering characterization was employed (Supplementary Fig. 6). Compared to the organic gel, the 1D WAXS data of PD-gel and PL-gel show increased peak intensity and significantly reduced half-peak width, confirming the enhancement of crystallization and crystal size during the ionic liquid salting-out process (Fig. 1f). At the same time, the 2D SAXS azimuthal integration curves of the PVA gel before and after the in situ localized alignment assisted salting-out process confirm the formation of a micro-oriented structure induced by the in situ fixation strategy (Supplementary Fig. 7). As shown in the 1D SAXS profiles, the peak position of the salting-out-only samples shifts toward higher q values, indicating a reduced average spacing between crystalline domains (Supplementary Fig. 8a, c). Notably, the localized alignment-assisted salting-out samples exhibit a further shift of the SAXS peak toward higher q values (Supplementary Fig. 8b, d), suggesting a more pronounced reduction in interdomain spacing and enhanced crystallinity. These results indicate that localized alignment effectively induces micro-orientation of polymer chains and promotes the formation of a denser and more ordered crystalline structure. This structural reorganization significantly contributes to the improved mechanical performance of the gel, as the aligned and enlarged crystalline domains serve as efficient load-bearing elements and energy dissipation centers, thereby enhancing the overall toughness of the material. XRD measurements were performed to analyze the crystalline structure of the three types of gels, and their degrees of crystallinity were calculated accordingly (Supplementary Fig. 9). Among them, the PL-gel exhibited the highest crystallinity at 54.0%, supporting the conclusion that localized alignment induced by fixed-orientation salting-out effectively promotes polymer chain alignment and crystallization. The tensile strength of the organic gel is 2.4 MPa, while PD-gel and PL-gel exhibit tensile strengths of 19.5 MPa and 26.2 MPa, respectively (8.3 and 11.1 times

that of the organic gel). Their toughness values are 109.5 MJ/m^3 and 123.7 MJ/m^3, which were 10.7 and 12.1 times that of the organic gel (10.3 MJ/m^3) respectively, surpassing most strategies reported in the literature (Fig. 1g, h). The compressive strength of the PL-gel also increased from 1.3 MPa for the organic gel to 12.4 MPa at 50% strain (Supplementary Fig. 10). Additionally, the tensile strength and toughness of PL-gel exceed those of PD-gel, highlighting the critical role of the synergistic effects of localized alignment and salting-out-induced entanglement in enhancing performance.

Design strategy for strengthening and toughening PVA ionic gel

To further understand the toughening effect of [Bmin]BF_4 on PVA organogels, different PL-gels were prepared using NaCl, NH_4SO_4, $C_6H_5Na_3O_7$, and [Bmin]BF_4 to assess the Hofmeister effect of [Bmin]BF_4 (Fig. 2a). Compared to conventional PVA salting-out agents, ionogels salted with the ionic liquid [Bmin]BF_4 exhibited the highest toughness (109.5 ± 10.9 MJ m^{-4}) and modulus (52.3 ± 9.4 MPa), as well as the greatest fracture strain (1012.5 ± 105.0%) and tensile strength (19.5 ± 1.5 MPa). This suggests that the interaction between the ionic liquid and PVA molecular chains is stronger, resulting in a more stable network structure (Fig. 2b, c). To clarify the influence of polymer concentration on the mechanical performance, we conducted additional experiments to determine the polymer concentration after the ionic liquid exchange. Since the total mass of polymer chains remains unchanged during the salting-out process, the polymer concentration (C_p) of the final PL-gel was estimated by measuring the mass of the gel before and after salting-out, using the following equation:

$$C_p = \frac{m_{organicgel} \times 18.4\%}{m_{PL-gel}} \quad (1)$$

where $m_{organicgel}$ is the total mass of the organic gel before salting-out, m_{PL-gel} is the total mass of the PL-gel after salting-out, and 18.4% represents the PVA content in the organic gel. The results show that the PL-gel possesses the highest polymer concentration among all tested samples. This is attributed to the synergistic effect of pre-

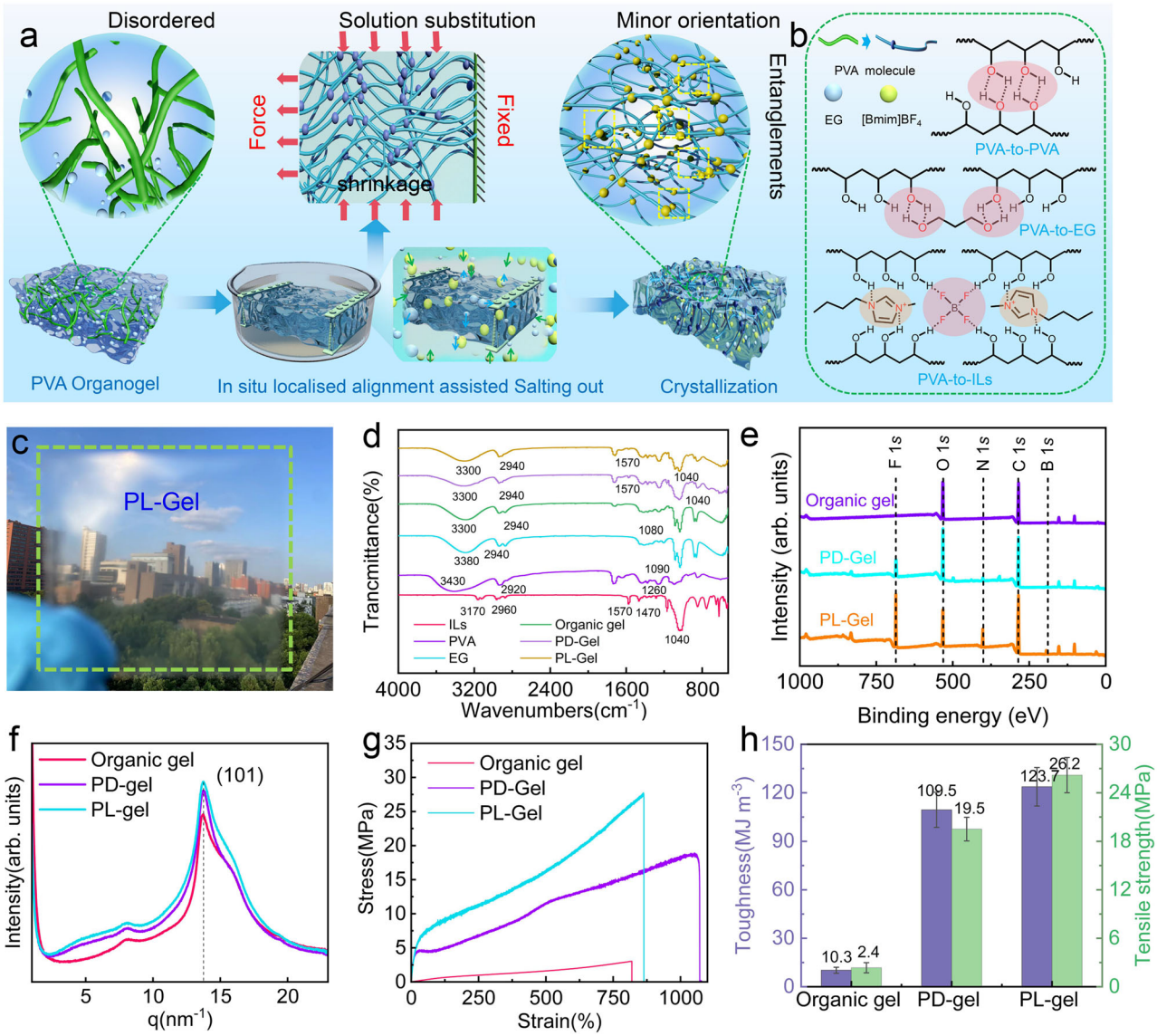

Fig. 1 | Preparation and mechanical properties of PL-gel. a Schematic illustration of the preparation process of PL-gel. **b** The intermolecular interactions between PVA, EG, and ILs. **c** Optical transparency of PL-gel samples. **d** FT-IR spectra of the ionic liquid, PVA, EG, organic gel, PD-gel, and PL-gel. **e** XPS spectra of the organic gel, PD-gel, and PL-gel. **f** 1D WAXS curves of the organic gel, PD-gel, and PL-gel. **g** Stress-strain curves of the organic gel, PD-gel, and PL-gel. **h** Comparison of toughness and tensile strength among the organic gel, PD-gel, and PL-gel. Data in (**h**) are presented as the mean ± SD from $n = 3$ independent samples.

https://doi.org/10.1038/s41467-025-63148-0

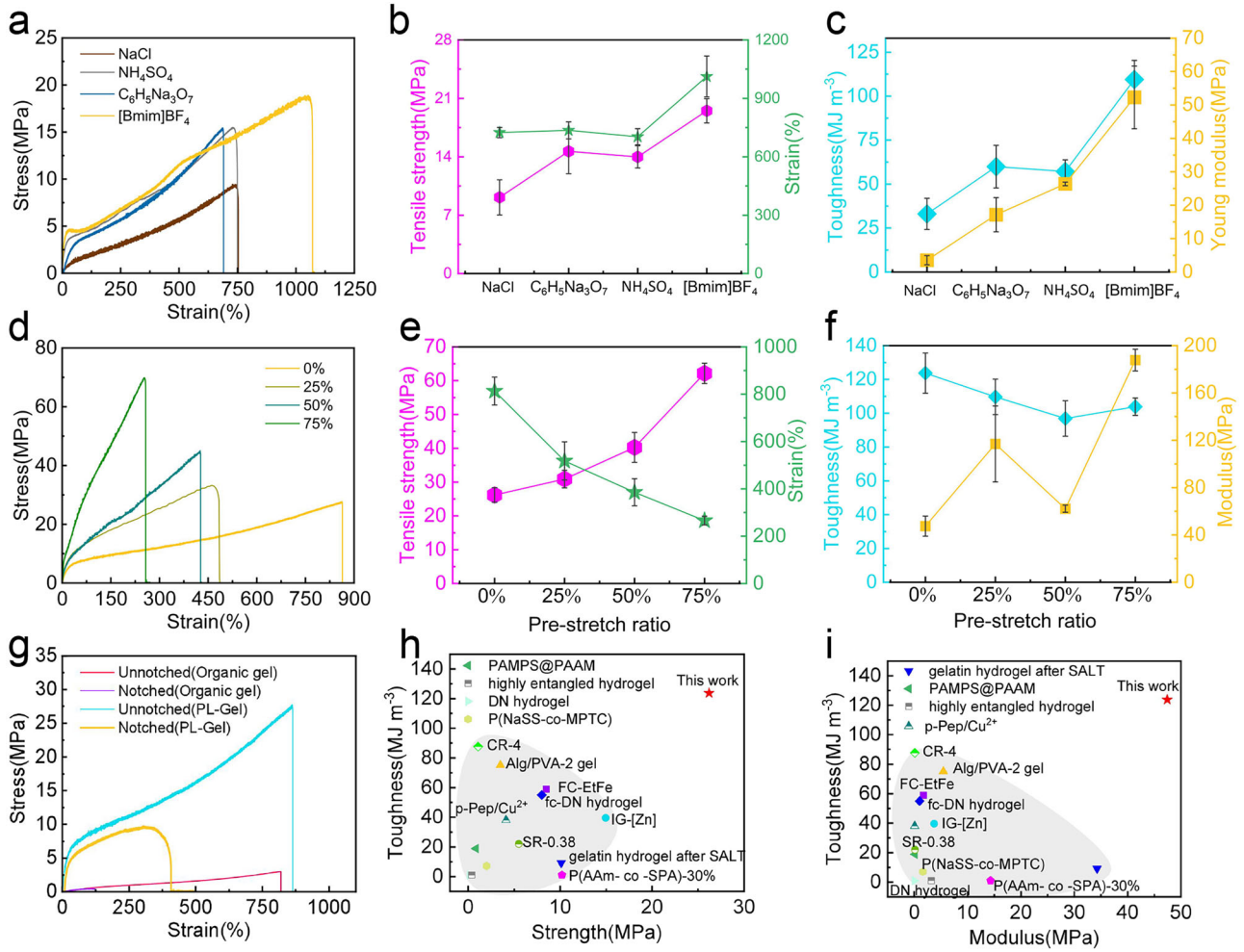

Fig. 2 | Design approaches for enhancing the strength and toughness of PVA ionic gels. a Tensile stress-strain curves of PVA organogels salted out with NaCl, NH_4SO_4, $C_6H_5Na_3O_7$, and [Bmin]BF_4. **b** Comparison of tensile strength and fracture strain. **c** Comparison of toughness and Young's modulus. **d** Tensile stress-strain curves of PL-gel pre-stretched to 0%, 25%, 50%, and 75%. **e** Comparison of tensile strength and fracture strain. **f** Comparison of toughness and Young's modulus. **g** Tensile stress-strain curves of organogel and PL-gel samples with and without notches. **h** Comparison of toughness and Young's modulus between PL-gel and other reported gels. **i** Comparison of toughness and tensile strength between PL-gel and other reported gels. Data in (**b**, **c**, **e**, **f**) are presented as their means ± SDs from n = 3 independent samples.

stretching and localized alignment salting-out, which facilitates solvent expulsion and promotes densification of the polymer network, thereby enhancing the mechanical strength (Supplementary Table 1).

Figure 2d compares the tensile stress-strain curves of PL-gels under various pre-stretching conditions. With increasing pre-stretching, the tensile stress of the ionogels significantly rises, while the fracture strain and toughness decrease accordingly (Fig. 2e, f). Pre-stretching design facilitates the formation of fibrous polymer chain structures in the ionogel, which increases the fracture stress. At the same time, the alignment of PVA chains limits further stretching of the fibrous structure due to pre-stretching, leading to premature fracture at lower strain levels. Images in Supplementary Fig. 11 show PD-gels and PL-gels before and after salting-out. PL-gels demonstrate no length changes after pre-stretching, with significant shrinkage in width and thickness, indicating that PVA chains are aligned along the stretching direction, forming an ordered, oriented structure. In contrast, PD-gels exhibit a curled structure due to non-uniform shrinkage in all three directions, suggesting a lack of chain alignment within the gel. Additionally, the mechanical performance of PL-gels salted for various durations (1, 4, 7, and 15 days) was also analyzed. As shown in Supplementary Fig. 12, prolonged salting-out time significantly enhances the strength, modulus, and toughness of the ionogels. Notably, a salting-out time of 7 days yields an optimal balance between polymer chain alignment and network densification. In contrast, prolonged salting-out for 15 days induces overstretching-related pre-strain, as evidenced which may adversely affect mechanical performance. The fracture property of PL-gel was further evaluated through pure shear tests (Fig. 2g, Supplementary Figs. 13 and 14). The fracture energy of the organogel was only 23.5 kJ m^{-2}, whereas the PL-gel exhibited a high fracture energy of 727.6 kJ m^{-2}, making it about 31 times greater than that of the organogel. The dense entanglement of polymer chains within the PL-gel alleviates stress concentration and effectively distributes the applied force across other chains, certifying that PL-gel is highly effective in preventing crack propagation.

To investigate the influence of ionic liquid content on the mechanical properties of the PL-gels, we performed a systematic study by immersing PVA gels with identical volume and composition in varying amounts of ionic liquid (100 mL, 200 mL, 300 mL, and 400 mL) during the salting-out process (Supplementary Fig. 15). As shown, increasing the volume of ionic liquid markedly enhances both the tensile strength and toughness of the resulting PL-gels. Notably, the gel treated with 400 mL of ionic liquid exhibits the highest tensile strength (~26 MPa) and elongation at break (~800%), in contrast to the one treated with 100 mL. These results suggest that a greater volume

https://doi.org/10.1038/s41467-025-63148-0

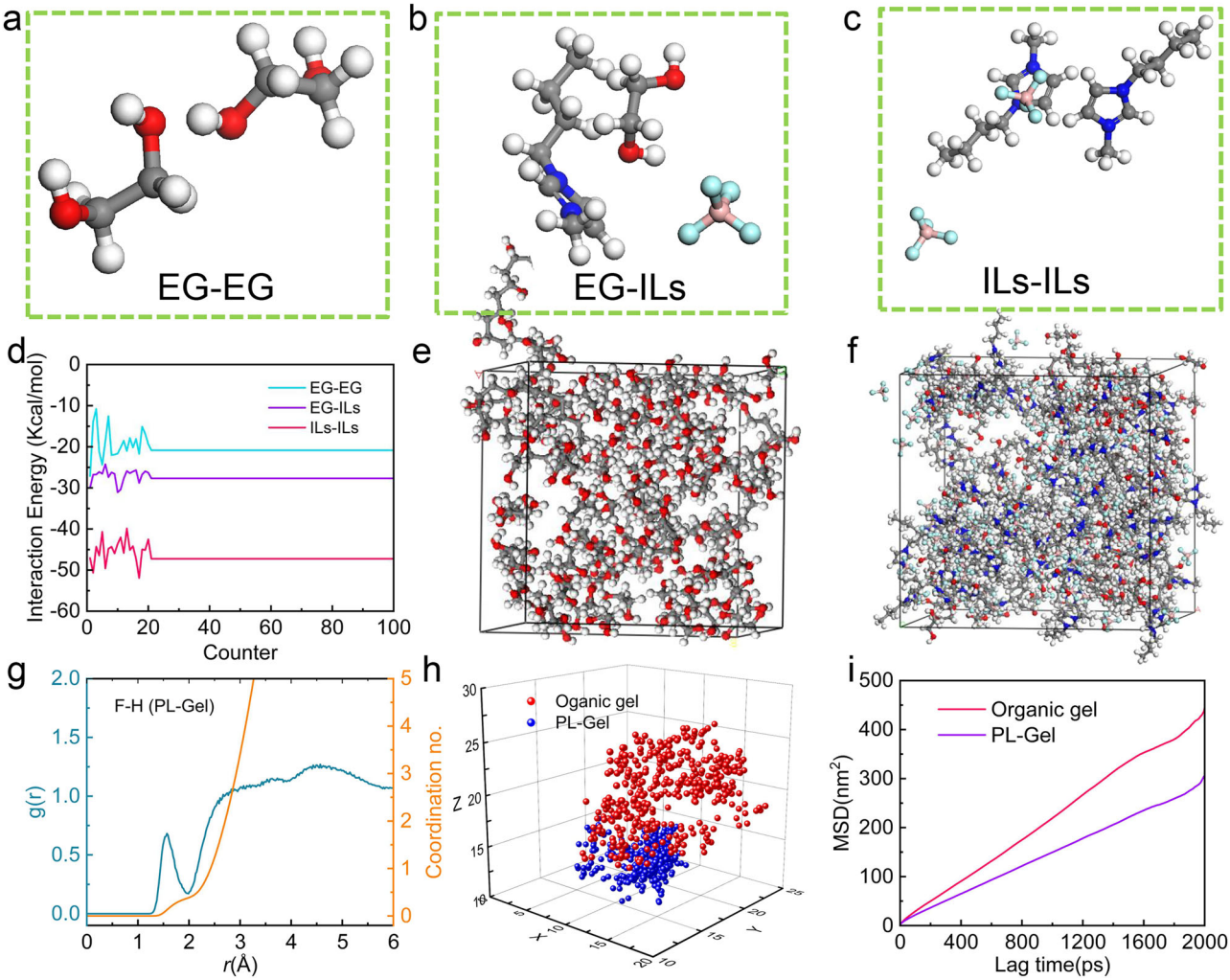

Fig. 3 | Strengthening mechanism of PVA ionic gel using molecular dynamics simulation. The molecular dynamics-optimized configurations of **a** EG-EG, **b** EG-ILs, and **c** ILs-ILs. **d** The interaction energies between EG-EG, EG-ILs, and ILs-ILs. **e** The molecular configurations of the organic gel in the molecular dynamics simulation. **f** The molecular configuration of the PL-gel in the simulation. **g** The radial distribution functions of F-H collected in the PL-gel. In the 1000 ps NVT analysis, the **h** trajectory and **i** mean square displacement (MSD) of EG in different gels. Color codes for atoms in (**a**–**c**, **e**, **f**): Gray, white, red, blue, cyan, and pink spheres represent carbon (C), hydrogen (H), oxygen (O), nitrogen (N), fluorine (F), and boron (B) atoms, respectively.

of ionic liquid facilitates more complete ion exchange and salting-out, thereby promoting polymer chain orientation and physical cross-linking. This structural reorganization significantly improves the mechanical performance of the gels. To evaluate the cyclic tensile performance of the ionic gel, 20-cycle tensile tests were conducted at strain levels of 10%, 20%, 30%, and 40% (Supplementary Fig. 16). The results reveal a gradual decline in mechanical strength and an increase in residual strain with higher deformation levels. For example, at 10% strain, the maximum stress decreased from 5.6 MPa to 4.6 MPa after 20 cycles, while at 40% strain, it dropped more substantially from 7.5 MPa to 4.8 MPa, accompanied by a residual strain of 22.79%. Although the cyclic durability is limited at large strains, this gel design prioritizes high strength and toughness, making it promising for applications where mechanical robustness is critical, while highlighting the need for further optimization for fatigue-resistance. The temperature-dependent mechanical properties of the gel were evaluated under both high- and low-temperature conditions (Supplementary Fig. 17). Within the typical temperature range of daily use, the gel maintains relatively stable mechanical performance. However, at elevated temperatures (60 °C), a noticeable decrease in tensile strength and a slight reduction in fracture strain were observed, likely due to thermal-induced structural relaxation (Supplementary Fig. 17a). In contrast, under low temperatures, the tensile strength remained stable at −30 °C and even slightly increased at −60 °C, while the fracture strain decreased significantly (Supplementary Fig. 17b), indicating restricted chain mobility and reduced ductility at lower temperatures. With ultra-high strength and extensibility, the toughness of the ionogel (121.9 MJ m^{-3}) surpasses that of previously reported tough ionogels and hydrogels by a considerable margin (Fig. 2h, i and Supplementary Table 2).

Comparative analysis and microstructural insights of strengthening mechanism

To further understand the role of ionic liquids in ionogels, a series of molecular dynamics analyses were carried out. Density functional theory (DFT) studies indicate that the binding energy for ILs-ILs interactions is −47.2 kcal/mol, while that for EG-ILs is −27.7 kcal/mol. Both values are lower than the binding energy of EG-EG interactions (−20.9 kcal/mol), suggesting that the introduction of ILs enhances the stability of the PVA gel networks (Fig. 3a–d). Additionally, the binding energy for PVA-ILs is −80.9 kcal/mol, significantly lower than that for PVA-EG (−21.1 kcal/mol), further confirming that ILs contribute to the stability of the PVA gel networks (Supplementary Fig. 18). To gain deeper insights into the microstructural properties of the gels, radial

https://doi.org/10.1038/s41467-025-63148-0

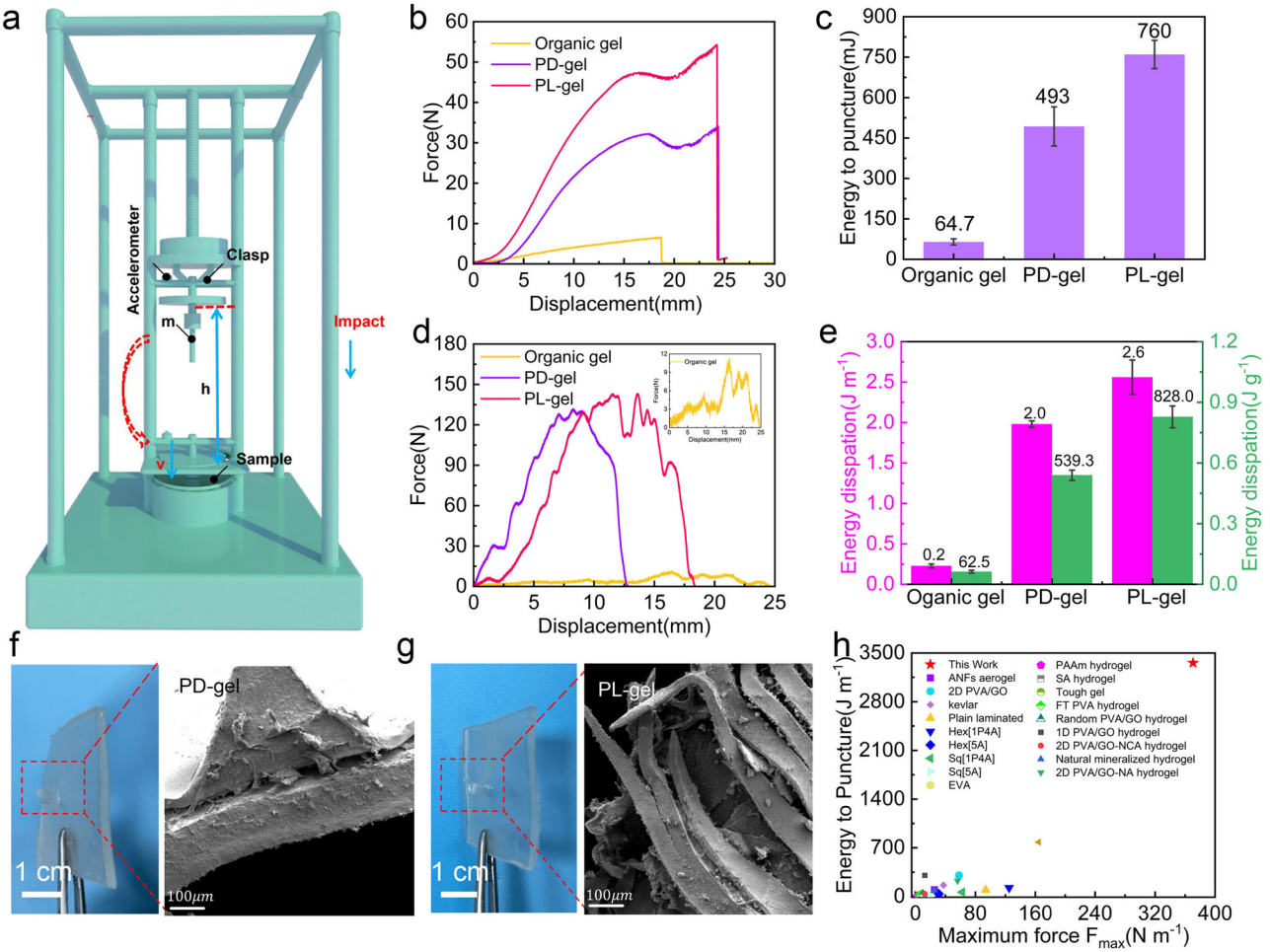

Fig. 4 | Puncture resistance performance. a Schematic illustration and images of the dynamic puncture test for PL-gel. **b** Quasi-static puncture force-displacement curves and **c** puncture energy for the organic gel, PD-gel, and PL-gel. **d** Dynamic puncture force-displacement curves and **e** quasi-static puncture energy for the organic gel, PD-gel, and PL-gel. Side view of **f** PD-gel and **g** PL-gel post-puncture, along with corresponding microstructural morphology of the fracture. **h** Comparison of the maximum puncture force and puncture energy of PL-gel with other reported gels[28–30]. Data in (**c**, **e**) are presented as the means ± SDs from $n = 3$ independent samples.

distribution function (RDF) and coordination number (CN) analyses on the gels before and after salting-out were performed (Fig. 3e, f). The RDF analysis of F-H interactions shows a peak at 1.6 Å, indicating the existence of hydrogen bonding between F and H (Fig. 3g). Similarly, the RDF for O-H interactions reveals a peak at 2.1 Å, proving the formation of hydrogen bonding between O and H (Supplementary Fig. 19). From the CN perspective, a decrease in the coordination number for O and H after salting-out was observed, while the coordination number for F with H increased (Fig. 3g). This reveals that F in the ionic liquid replaces O in EG, forming stronger hydrogen bonds with H, thereby enhancing the overall stability of the material. Supplementary Fig. 20 presents the hydrogen bond analysis, including statistics on different hydrogen bond lengths and angles. On one hand, the fluorine (F) within the gel replaces oxygen (O) to form more hydrogen bonds with hydrogen (H), leading to an overall increase in hydrogen bond quantity. On the other hand, the distribution of bond lengths shows that F-H bonds are shorter, which corresponds to stronger hydrogen bonding interactions. This change indicates that the formation of F-H hydrogen bonds not only increases the number of hydrogen bonds but also strengthens them, thus enhancing the structural. As shown in Fig. 3h, the diffusion region of ethylene glycol (EG) in the ionogel becomes smaller after salting-out. Ionic liquids form a hydrogen-bonding network with EG and polymer chains, restricting the movement of the EG network and increasing the likelihood of mutual constraint among polymer molecules. Furthermore, the reduced diffusion coefficient after salting-out (Fig. 3i) indicates enhanced intermolecular interactions, leading to tighter interactions between molecular chains and a more stable overall structure.

Puncture resistance performance

In the fields of construction engineering, aerospace, and protective equipment, it is crucial for materials to maintain structural integrity and mechanical performance under high stress and extreme environments. Among these properties, puncture resistance is a key factor that enables materials to effectively withstand extreme loads from external sources, preventing structural failure and ensuring stability and safety under harsh conditions. Thus, quasi-static puncture tests were firstly conducted to evaluate the puncture resistance of the materials (Supplementary Fig. 21). The maximum puncture force of PL-gel significantly increased from 32.0 ± 2.7 N for PD-gel to 57.9 ± 4.0 N under quasi-static conditions, which is 9.1 times that of the untreated organic gel (Fig. 4b). Additionally, the puncture energy increased from 493 ± 72 mJ for PD-gel to 760 ± 52 mJ (PL-gel), which is 11.8 times that of the untreated organic gel (Fig. 4c). To comprehensively assess the puncture resistance of PL-gel, dynamic puncture tests were also performed (Fig. 4a). The results showed that among the three different PVA gels, PL-gel could withstand a maximum puncture force of 139.7 ± 12.3 N and a puncture energy of 2.6 ± 0.2 J/

https://doi.org/10.1038/s41467-025-63148-0

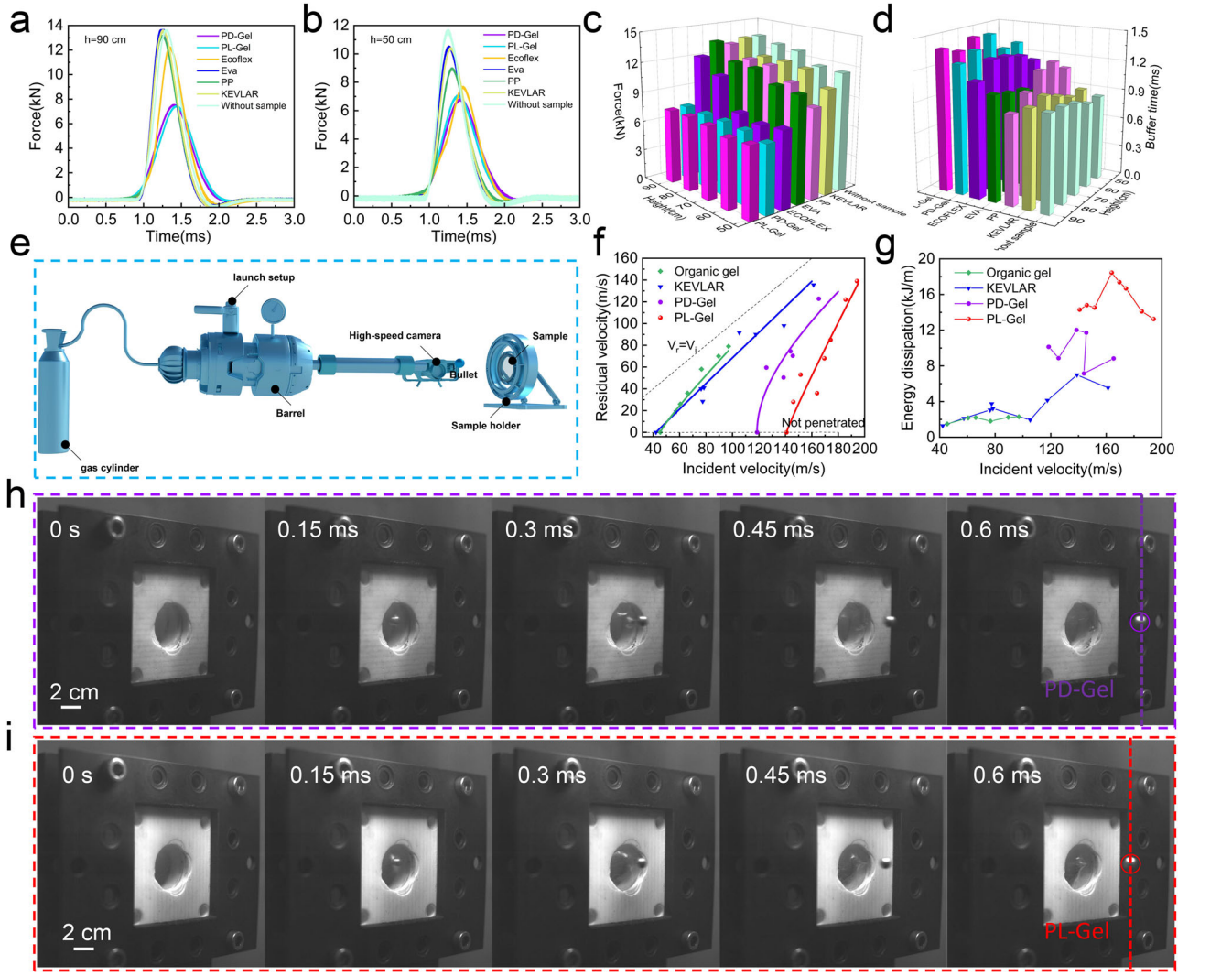

Fig. 5 | Impact resistance and energy dissipation capability. Force-time curves of PL-gel, Ecoflex, EVA foam, and PP at a drop height of **a** 90 cm and **b** 50 cm. **c** Peak force values and **d** cushioning time of different samples collected from the above experiments. **e** Schematic diagram of the ballistic impact testing system. **f** Impact velocity of aluminum projectiles after passing through organic gel, PD-gel, PL-gel, and Kevlar. **g** Energy dissipation of samples at different impact velocities. Impact process of **h** PD-gel at an initial velocity of 181.5 m/s and **i** PL-gel at an initial velocity of 179.9 m/s.

m, significantly surpassing both the untreated organic gel and PD-gel (Fig. 4d, e). This further validates the reliable performance of PL-gel under extreme dynamic loads, highlighting its potential application value in construction, aerospace, and protective equipment. Furthermore, Fig. 4f, g illustrate that the fracture surface of PL-gel exhibits noticeable fiber pull-out, confirming the impact of the micro-oriented structure formed by localized alignment assisted salting-out on the material's toughness. Figure 4h compares the maximum puncture force and puncture energy of PL-gel with those of existing conventional materials, indicating that PL-gel has higher quasi-static impact resistance than synthetic gels such as ANFs aerogel, 2D PVA/GO, and Hex[1P4A].

Impact resistance and energy dissipation capability

In everyday applications, materials frequently encounter various low-velocity impact scenarios, such as collisions during the handling of construction components, cushioning materials mitigating minor drops, or low-speed vehicle impacts on safety structures. To evaluate the protective performance of PL-gel under low-velocity impact conditions, this study designed a drop hammer test to simulate the material's performance in typical cushioning applications. Figure 5a, b and Supplementary Fig. 16 illustrate the force-time curves for PD-gel, PL-gel, Ecoflex, and other samples as the drop height increased from 50 cm to 90 cm. It is evident that under impacts from 50 to 90 cm, PL-gel outperformed EVA foam and PP in terms of peak force and cushioning time. Even in comparison to Ecoflex, PL-gel demonstrated exceptional damping effectiveness. Figure 5c, d further compare the peak force and cushioning time, with PL-gel reaching a peak force of 7.5 kN and a cushioning time of 1.2 s at a 90 cm drop height. Compared to the control group Ecoflex and the no-sample condition, PL-gel reduced the peak force by 40% and 45%, respectively. In aerospace and protective equipment fields, materials must withstand high-velocity impact loads, such as the impact of an aircraft crash, the ballistic resistance of tactical gear, or the protection against high-speed debris and explosive impacts in defense structures. Under these extreme conditions, a material's impact resistance is crucial. To investigate this potential, ballistic impact testing was conducted on the tough ionic gel (Fig. 5e). A spherical projectile was launched at the sample using an air gun under controlled pressure. As shown in Fig. 5f, the relationship between the projectile's initial velocity (V_i) and residual velocity (V_r) follows the Recht-Ipson formula:

$$v_r = k(v_i^n - v_b^n)^{\frac{1}{n}} \quad (2)$$

https://doi.org/10.1038/s41467-025-63148-0

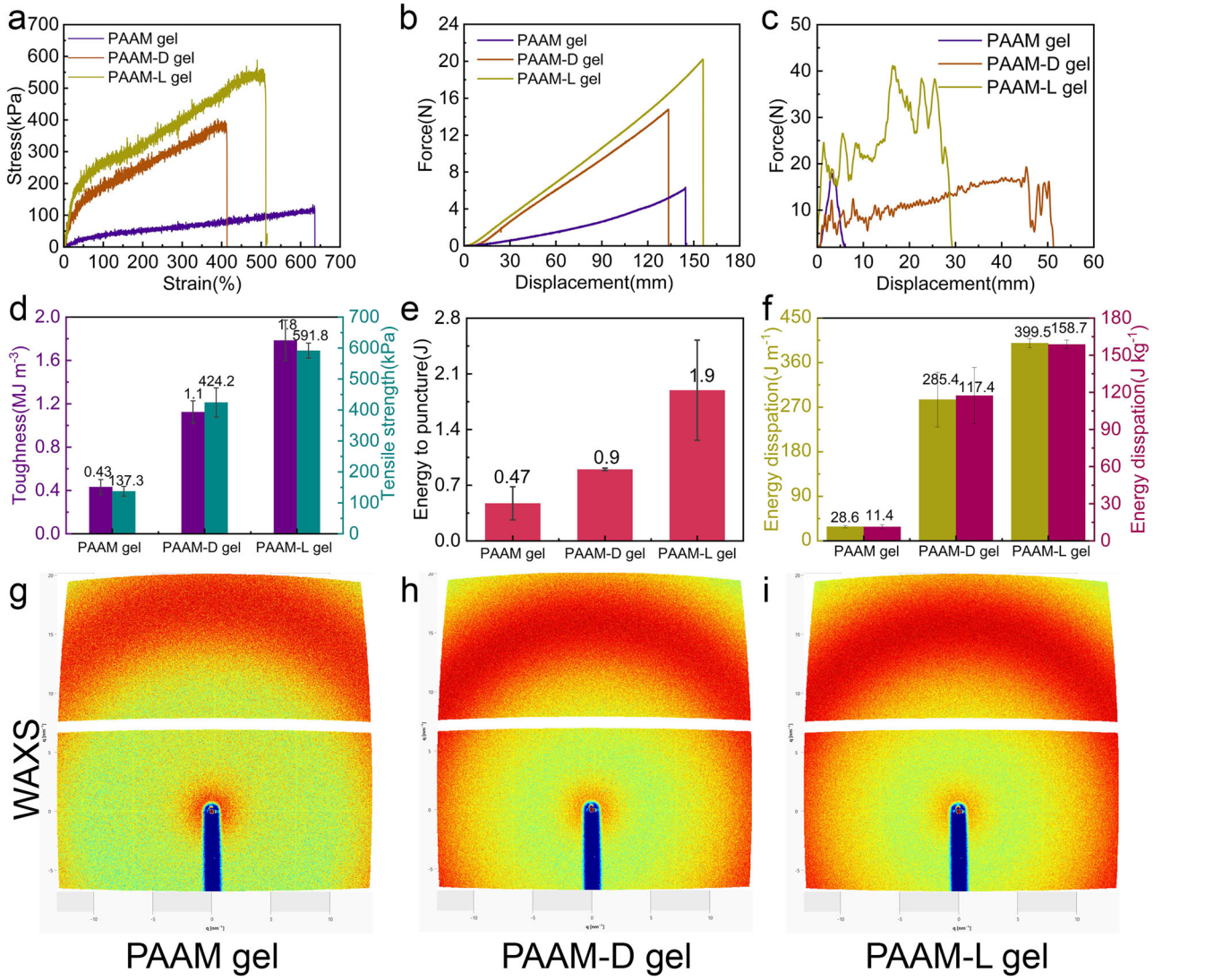

Fig. 6 | Universality and customizability of the localized alignment assisted salting-out strategy. a Stress-strain curves of PAAM hydrogel, PAAM-D gel, and PAAM-L gel. **b** Quasi-static puncture force-displacement curves of PAAM hydrogel, PAAM-D gel, and PAAM-L gel. **c** Dynamic puncture force-displacement curves of PAAM hydrogel, PAAM-D gel, and PAAM-L gel. **d** Comparison of toughness and tensile strength among PAAM hydrogel, PAAM-D gel, and PAAM-L gel. **e** Quasi-static puncture energy of PAAM hydrogel, PAAM-D gel, and PAAM-L gel. **f** Dynamic puncture energy of PAAM hydrogel, PAAM-D gel, and PAAM-L gel. **g**–**i** 2D WAXS models of PAAM hydrogel, PAAM-D gel, and PAAM-L gel. Data in (**d**–**f**) are presented as the means ± SDs from $n = 2$–3 independent samples.

where k and n are material-specific constants, and V_b represents the critical velocity at which $V_r = 0$ m/s. As shown in Fig. 5g, PL-gel exhibited a significantly higher critical velocity ($V_b = 141.0$ m/s) compared to the other three materials. This result demonstrates that PL-gel possesses effective penetration resistance under high-velocity impact conditions, highlighting its potential in extreme protection applications. The energy dissipation (ΔE) of the sample was calculated as follows:

$$\Delta E = \frac{m(v_i^2 - v_r^2)}{2t} \quad (3)$$

where m is the mass of the projectile (0.7 g), and t is the thickness of the sample (0.5 mm). The results indicate that at an impact velocity of 163.9 m/s, PL-gel achieved an extraordinary ΔE of 18.44 kJ/m, which is 3.3 times that of Kevlar at a similar impact speed (Fig. 5g). Under similar impact velocities, the residual velocity of the projectile after penetrating the PL-gel was markedly lower than that observed for the PD-gel (Fig. 5h, i). This finding further confirms that the high degree of aggregation, strong entanglement, and crystallinity induced by the localized alignment assisted salting-out process effectively enhance the material's anti-penetration performance under high-speed impacts.

Generality and customizability of localized alignment assisted salting-out strategy

By adopting a localized alignment assisted salting-out strategy, its applicability to other molecular chains and solvents was further evaluated. Replacing the molecular chain from PVA to PAAM and changing the solvent from ethylene glycol to water, PAAM-L gel with enhanced mechanical strength was successfully fabricated. Compared to untreated PAAM hydrogels, PAAM-L gel exhibited approximately 4.31-fold increase in strength (591.8 ± 24.3 kPa) and 4.14-fold increase in toughness (1.8 ± 0.2 MJ/m^3) (Fig. 6a, d). Given the enhanced mechanical properties of PAAM-L gel, its puncture resistance was proceeded to test (Fig. 6b, e). The results indicated substantial improvements in both maximum puncture force and puncture energy under quasi-static and dynamic puncture conditions. PAAM-L gel achieved a quasi-static puncture energy of 1.9 ± 0.6 J, 4.0 times that of the PAAM hydrogel, while its dynamic puncture energy reached 399.5 ± 9.0 J/m, 14.0 times

that of the PAAM hydrogel (Fig. 6c, f). These results further confirm the versatility of the in situ localized alignment assisted salting-out strategy in improving the performance of gels (Fig. 6g–i). Compared to the PAAM hydrogel and PAAM-D gel, the 1D WAXS data of the PAAM-L gel shows a noticeable shift of the broad peak toward lower q-values and a slight increase in peak intensity (Supplementary Fig. 23). This shift brings the scattering signal closer to the amorphous halo observed in the pure ionic liquid (Supplementary Fig. 24), suggesting that the localized alignment assisted salting-out treatment leads to enhanced ion–polymer interactions or local structural rearrangements. Additionally, leveraging the high strength and excellent stretchability of PAAM-L gel, the ease of customizing its additional functionalities, such as conductivity, were also demonstrated to meet diverse application needs (Supplementary Fig. 25). This adaptability makes it suitable for real-time human motion monitoring and detecting various physiological signals. These findings highlight the localized alignment assisted salting-out strategy as a highly versatile toughening method that allows for simple customization of desired properties across different materials. This approach not only enhances mechanical performance but also provides diversified application potential.

Discussion

In this study, we have successfully developed a approach to enhancing the mechanical properties and impact resistance of ionic gels. By combining ionic liquids with a localized alignment assisted salting-out process, we have achieved a highly ordered, micro-oriented structure within polyvinyl alcohol (PVA) gels, resulting in significantly improved tensile strength, toughness, and modulus. The resulting PL-gels not only exhibit enhanced mechanical performance, including high puncture force and energy dissipation, but also demonstrate exceptional impact resistance, surpassing conventional materials like Kevlar under similar impact conditions. Moreover, molecular dynamics simulations confirm the role of enhanced hydrogen bonding and chain interactions in stabilizing the gel's structure, contributing to its enhanced mechanical performance. Importantly, the localized alignment assisted salting-out strategy has shown broad applicability, extending its benefits to other polymer matrices such as PAAM hydrogels. This work presents a promising pathway for the development of high-performance, impact-resistant materials suitable for a wide range of advanced applications, from flexible electronics to protective gear and aerospace technologies, providing enhanced reliability and safety in extreme environments.

Methods

Materials

Ethylene glycol (EG), sodium chloride (NaCl, AR), ammonium sulfate ($(NH_4)_2SO_4$, AR), trisodium citrate dihydrate ($Na_3C_6H_5O_7{\cdot}2H_2O$, AR), and ammonium persulfate (APS, AR) were purchased from Sinopharm Chemical Reagent Co., Ltd. Polyvinyl alcohol (PVA, Mw ~205,000), 1-butyl-3-methylimidazolium tetrafluoroborate (ionic liquid, ≥97%), acrylamide (AM, AR, ≥99%), and N,N′-methylenebis (acrylamide) (MBAA, 99%) were obtained from Aladdin Industrial Corporation (Shanghai, China).

Fabrication of PVA Organogels

To prepare the PVA organogels, 25 g of polyvinyl alcohol (PVA, Mw~205,000) was dissolved in 100 mL of ethylene glycol by stirring at 130 °C for 3 h. The resulting homogeneous mixture was then cast into a custom-made polytetrafluoroethylene (PTFE) mold and frozen at −20 °C for 12 h to obtain the PVA organogel.

Fabrication of PVA Ionic Gels

The PVA organogels were then immersed in 1-butyl-3-methylimidazolium tetrafluoroborate for seven days to perform ion exchange, resulting in high-strength and tough direct salting-out PVA ionic gels, referred to as PD-gels. Here, "P" stands for polyvinyl alcohol (PVA), and "D" denotes the direct salting-out process. Additionally, the PVA organogels were immersed in equal volumes of saturated aqueous solutions of sodium chloride, ammonium sulfate, and trisodium citrate for seven days to perform ion exchange, producing PVA ionic gels obtained through direct salting-out using different salt solutions. Furthermore, by pre-stretching the PVA organogels to different extents (0%, 25%, 50%, and 75%) and fixing them onto PU plates before performing the same ion exchange process, high-strength and tough in situ localized alignment assisted salting-out PVA ionic gels, referred to as PL-Gels, were obtained. Similarly, by fixing the PVA organogel onto a PU plate and immersing it in 1-butyl-3-methylimidazolium tetrafluoroborate solution for different durations (1 day, 4 days, 7 days, and 14 days), PVA ionic gels with varying salting-out times were obtained. (Supplementary Table 3).

Fabrication of PAAM Hydrogels

For the preparation of PAAM hydrogels, 96 g of acrylamide, 0.2 g of N, N′-methylenebisacrylamide, and 0.08 g of ammonium persulfate were dissolved in 300 mL of deionized water with stirring at room temperature. The resulting mixture was cast into a custom-made PTFE mold and heated at 60 °C for 3 h to obtain PAAM hydrogels. These hydrogels were then subjected to the same ion exchange procedure to produce PAAM direct-salting-out and localized alignment assisted salting-out ionic gels.

Characterization

Microscopic Structure Analysis: The microstructure of the PVA gels was examined using a scanning electron microscope (SEM, Gemini 500, Carl Zeiss Jena, Germany).

Chemical Structure Analysis: Fourier-transform infrared (FTIR) spectroscopy was performed using a Nicolet iN10 infrared microscope (Thermo Scientific, USA) in ATR mode over a range of 4000–500 cm^{-1} to analyze the chemical structure. X-ray photoelectron spectroscopy (XPS, Thermo Scientific ESCALAB 250Xi) was employed to further analyze the elemental composition.

Optical Transparency Measurement: The transmittance of the PVA gels was measured using a UV-Vis-NIR spectrophotometer (Solid 3700, Shimadzu, Japan).

Thermal Stability Analysis: The thermal stability of the PVA gels was assessed using thermogravimetric analysis (TGA Q5000IR, TA, USA), where samples were heated from 30 °C to 800 °C at a rate of 10 °C/min under a nitrogen atmosphere.

X-ray Scattering Analysis: To investigate the internal structural differences among samples, wide-angle and small-angle X-ray scattering (WAXS and SAXS) measurements were performed using a SAXSpoint 2.0 system (Anton Paar GmbH, Austria) equipped with a Cu Kα radiation source (λ = 1.54 Å). The sample-to-detector distance was set to 113 mm, and all measurements were conducted under vacuum to eliminate air scattering. The 2D data were converted to 1D profiles [I(q) ~q plot] using Fit2D software, where I is the scattering intensity, and q is the scattering vector [$q = 4\pi\sin\theta/\lambda$, where 2θ is the scattering angle and λ is the X-ray wavelength]. To ensure comparability among different samples, the thickness of each gel sample was carefully controlled at approximately 0.5 mm to minimize variability. To correct for potential differences in X-ray transmittance, we processed the raw scattering images using the image calculator function in Saxsanalysis software and applied transmittance correction as follows:

$$I_{corr} = \frac{I_S}{T_S} \tag{4}$$

where I_S is the measured scattering intensity and T_S is the transmittance of the sample. In SAXS measurements, the fixed chain alignment direction was set along the horizontal axis (x-axis) in the 2D scattering

patterns. Azimuthal integration at $q = 0.7\,nm^{-1}$ was performed to evaluate the degree of orientation. All 2D SAXS images are displayed with appropriate scale bars to clarify the spatial features of the scattering patterns.

Mechanical Testing: Tensile and compression tests were carried out on an MTS machine (MTS Standard 43) at a strain rate of $0.005\,s^{-1}$. The PVA gel samples for tensile tests were prepared in dimensions of $60 \times 10 \times 0.5\,mm^3$, and those for compression tests were $20 \times 20 \times 2\,mm^3$. Samples for pure shear tests had a thickness of 0.25 mm and a width of 10 mm, with a fixed clamping distance of 3 cm. For samples with notches cut from the center of the clamps, the cutting width was 1 mm. The fracture energy of the gels was calculated by dividing the work done within the critical stretch range on unnotched samples by the cross-sectional area.

Puncture and Impact Testing: Quasi-static puncture tests were performed on an MTS machine using a hemispherical probe (diameter: 4 mm) approaching the sample center at a constant speed of 10 μm/s until penetration. To investigate the energy dissipation properties, a drop-weight apparatus equipped with force and acceleration sensors was employed. Samples with dimensions of $20 \times 20 \times 2\,mm^3$ were subjected to impact from various heights. The thickness of the PVA gels was measured using a digital micrometer (Mitutoyo, 0–25 mm). For high-velocity projectile impact tests, an aluminum projectile (diameter: 8 mm, mass: 0.7 g) was fired from a pneumatic gun. The initial velocity was measured using a laser velocimeter mounted at the gun muzzle. The gel samples were clamped to a steel frame, exposing a circular area with a diameter of 30 mm. The damage process and residual velocity of the projectile passing through the PVA gels were recorded with a high-speed camera.

Electrical Performance Testing: The external electrical signal of the PAAM gels under external stimuli was recorded using a ModuLab test system (Solartron Analytical, AMETEK Advanced Measurement Technology) with an applied voltage of 3 V.

Molecular dynamics simulations: Molecular dynamics simulations were conducted using the commercial software Materials Studio, employing the Compass force field to model atomic interactions among PVA chains, EG molecules, and ionic liquid molecules. For the PVA organogel, two PVA chains (each composed of 20 monomers) were placed in a box containing EG molecules. For the ionic gel post-salting-out, 100 ethanol molecules were also added to the box. The initial simulation unit cell dimensions were set to 23.7 Å × 23.7 Å × 23.7 Å, with lattice parameters $\alpha = \beta = \gamma = 90°$. Energy minimization was performed for each configuration until convergence was achieved, followed by molecular dynamics (MD) calculations using the NVT ensemble. The simulation lasted for 200 ps with a step size of 1 fs at a temperature of 298 K.

Interaction energy: The interactions studied included EG with ionic liquids, EG with EG, and ionic liquids with each other. Subsequently, PVA molecules were introduced to assess their impact on the gel system, specifically focusing on PVA-EG and PVA-IL interactions. The interaction energy (E_{int}), which quantifies the strength of interactions among the system components, is calculated using the following formula:

$$E_{int} = E_{total} - \sum E_{components} \quad (5)$$

where E_{total} and $E_{component}$ represent the total energy of the system and the energy of each individual component, respectively. Negative values of E_{int} indicate stable adsorption between components, with a more negative E_{int} reflecting a stronger interaction within the system.

Data availability

All relevant data generated from this study are available from the article and Supplementary Information, or available from the corresponding authors upon request. The other relevant source data are available at https://doi.org/10.6084/m9.figshare.29649170.v2. Source data are provided with this paper.

References

1. He, X. et al. Highly conductive and stretchable nanostructured ionogels for 3D printing capacitive sensors with superior performance. *Nat. Commun.* **15**, 6431 (2024).
2. Sun, B., Liu, K., Wu, B., Sun, S. & Wu, P. Low-hysteresis and tough ionogels via low-energy-dissipating cross-linking. *Adv. Mater.* **36**, 2408826 (2024).
3. Wang, M. et al. Glassy gels toughened by solvent. *Nature* **631**, 313–318 (2024).
4. Zhu, Y. et al. A general strategy for synthesizing biomacromolecular ionogel membranes via solvent-induced self-assembly. *Nat. Synth.* **2**, 864–872 (2023).
5. Ma, C. et al. Highly processable ionogels with mechanical robustness. *Adv. Funct. Mater.* **33**, 2211771 (2023).
6. Shen, Z., Zhu, X., Majidi, C. & Gu, G. Cutaneous ionogel mechanoreceptors for soft machines, physiological sensing, and amputee prostheses. *Adv. Mater.* **33**, 2102069 (2021).
7. Wang, J. et al. High-resolution flexible iontronic skins for both negative and positive pressure measurement in room temperature wind tunnel applications. *Nat. Commun.* **15**, 7094 (2024).
8. Peng, W. et al. A strong and tough ion-gel enabled by hierarchical meshing and ion hybridizations collaboration. *Adv. Funct. Mater.* **35**, 2414682 (2025).
9. Wang, M. et al. Tough and stretchable ionogels by in situ phase separation. *Nat. Mater.* **21**, 359–365 (2022).
10. Cao, K. et al. Bio-inspired multiscale design for strong and tough biological ionogels. *Adv. Sci.* **10**, 2207233 (2023).
11. Matsuda, T., Kawakami, R., Namba, R., Nakajima, T. & Gong, J. P. Mechanoresponsive self-growing hydrogels inspired by muscle training. *Science* **363**, 504–508 (2019).
12. Li, X. et al. Role of hierarchy structure on the mechanical adaptation of self-healing hydrogels under cyclic stretching. *Sci. Adv.* **9**, eadj6856 (2023).
13. Jin, J.-N. et al. Mechanical training enabled reinforcement of polyrotaxane-containing hydrogel. *Angew. Chem. Int. Ed.* **62**, e202218313 (2023).
14. Ye, Y. et al. Ultrastretchable ionogel with extreme environmental resilience through controlled hydration interactions. *Adv. Funct. Mater.* **33**, 2209787 (2023).
15. Ye, Y., Zhang, Y., Chen, Y., Han, X. & Jiang, F. Cellulose nanofibrils enhanced, strong, stretchable, freezing-tolerant ionic conductive organohydrogel for multi-functional sensors. *Adv. Funct. Mater.* **30**, 2003430 (2020).
16. Li, X. et al. Superstrong ionogel enabled by coacervation-induced nanofibril assembly for sustainable moisture energy harvesting. *ACS Nano* **18**, 12970–12980 (2024).
17. Yao, X. et al. Solvent-adaptive hydrogels with lamellar confinement cellular structure for programmable multimodal locomotion. *Nat. Commun.* **15**, 9254 (2024).
18. Peng, L. et al. One-dimensionally oriented self-assembly of ordered mesoporous nanofibers featuring tailorable mesophases via kinetic control. *Nat. Commun.* **14**, 8148 (2023).
19. Wang, Y. et al. Highly compressible and environmentally adaptive conductors with high-tortuosity interconnected cellular architecture. *Nat. Synth.* **1**, 975–986 (2022).
20. Wu, S. et al. Spider-silk-inspired strong and tough hydrogel fibers with anti-freezing and water retention properties. *Nat. Commun.* **15**, 4441 (2024).

21. Ren, J. et al. Super-tough, non-swelling zwitterionic hydrogel densor based on the hofmeister effect for potential motion monitoring of marine animals. *Adv. Mater.* **36**, 2412162 (2024).
22. Wu, S. et al. Poly(vinyl alcohol) hydrogels with broad-range tunable mechanical properties via the hofmeister effect. *Adv. Mater.* **33**, 2007829 (2021).
23. Hua, M. et al. Strong tough hydrogels via the synergy of freeze-casting and salting out. *Nature* **590**, 594–599 (2021).
24. Mredha, M. T. I. et al. A facile method to fabricate anisotropic hydrogels with perfectly aligned hierarchical fibrous structures. *Adv. Mater.* **30**, 1704937 (2018).
25. Dupont, J. et al. Ionic liquids in metal, photo-, electro-, and (bio) catalysis. *Chem. Rev.* **124**, 5227–5420 (2024).
26. Gao, S. et al. Design principles and applications of ionic liquids for transdermal drug delivery. *Adv. Sci.* **11**, 2405983 (2024).
27. Sun, H., Qi, J., Yu, K. & Yin, J. Research progress of ionic liquids for supercapacitor electrolytes. *N. Chem. Mater.* **52**, 13–17 (2024).
28. Wu, J. et al. Acid-assisted toughening aramid aerogel monoliths with ultralow thermal conductivity and superior tensile toughness. *Adv. Funct. Mater.* **34**, 2307072 (2024).
29. Liang, X. et al. Impact-resistant hydrogels by harnessing 2D hierarchical structures. *Adv. Mater.* **35**, 2207587 (2023).
30. Yin, Z., Hannard, F. & Barthelat, F. Impact-resistant nacre-like transparent materials. *Science* **364**, 1260–1263 (2019).

Acknowledgements

This work was supported by the National Natural Science Foundation of China (Grant Nos. 12202435 to M.S., 12132016, 12427802 and 52321003 to X.G.) and the Fundamental Research Funds for the Central Universities (Grant No. WK2090000060 to M.S.). This study was also supported by the USTC Center for Micro and Nanoscale Research and Fabrication.

Author contributions

X.G. and M.S. designed and supervised the whole project. Z.Z. and M.S. developed the composites and completed the experiments. Z.Z. and M.S. analyzed the data and wrote the manuscript. Z.L., Y.P., J.W., and S.D. assisted in the conduct of experiments. All the authors were actively involved in discussion, analysis, and revision.

Competing interests

The authors declare no competing interests.

Additional information

Supplementary information The online version contains supplementary material available at https://doi.org/10.1038/s41467-025-63148-0.

Correspondence and requests for materials should be addressed to Min Sang or Xinglong Gong.

Peer review information *Nature Communications* thanks Hongzan Song and the other, anonymous, reviewers for their contribution to the peer review of this work. A peer review file is available.